Torsional Dynamics Compensation Enhances Robotic Control of Tip-Steerable Needles

John P. Swensen and Noah J. Cowan

Abstract— **Needle insertions serve a critical role in a wide variety of medical interventions. Steerable needles provide a means by which to enhance existing percutaneous procedures and afford the development of entirely new ones. Here, we present a new time-varying model for the torsional dynamics of a steerable needle, along with a new controller that takes advantage of the model. The torsional model incorporates time-varying mode shapes to capture the changing boundary conditions caused during insertion of the needle into the tissue. Extensive simulations demonstrate the improvement over a model that neglects torsional dynamics and illustrates the possible effect of torsional model order on efficacy. Pilot feedback control experiments, conducted in artificial tissue (plastisol) under stereo image guidance, validate the overall approach: our results substantially out-perform previously reported experimental results on controlling tip-steerable needles.**

I. INTRODUCTION

Percutaneous interventions play a critical role in modern medicine. Despite the ubiquity of needle-based procedures, clinical needle interventions are largely based on Alexander Wood's nineteenth century idea: delivery therapy subcutaneously through the lumen of sharp, stiff tubes [18]. There have been many new and exciting integrated systems for deploying needles, but remarkably little advancement in the needle insertion mechanism itself until recently (see [2], [11] for a review). Notwithstanding these research advances, clinical interventions continue to rely primarily on straight insertion of steel needles. Recent exploration into steerable needles shows promise to improve existing procedures and help devise new procedures as needle steering improves [2].

In this paper, we derive and demonstrate a new model for torsional dynamics which we couple with an existing kinematic model of tip-steerable needles [16]. The primary purpose of the additional modeling of torsion is to improve the estimation and control of the needle tip; here we perform control to a plane during continuous insertion for comparison to previous work [7]. The previous modeling and control of tip-steerable needles makes the assumption that the insertion and rotational velocities at the tip of the needle are equivalent to those at the base of the needle. However, twisting a long slender beam from the controlled proximal end will result in torsional windup along the length of the needle. This realization motivates this development of a system model that incorporates the torsional dynamics, such that an automatic feedback controller can be designed to compensate accordingly.

This work was supported by the National Institutes of Health under grant R01-EB006435.

N.J. Cowan is with the Department of Mechanical Engineering, Johns Hopkins University, Baltimore, MD 21218, USA ncowan@jhu.edu

J.P. Swensen is with the Department of Mechanical Engineering, Johns Hopkins University, Baltimore, MD 21218, USA jpswensen@jhu.edu

A. Related work

The foundational papers of DiMaio et al. [3], Okazawa et al. [9], and Webster et al. [16] have changed the landscape of percutaneous therapies into a "post Wood era", at least insofar as research is concerned. DiMaio and Salcudean [3] were the first to investigate the complex interaction between robotically controlled needles and simulated tissues. Okazawa et al. [9] provided the first known mechanism design for affecting needle motion inside tissue by engineering the needle itself; their design consisted of an outer straight tube and inner stylet with a preset fixed radius of curvature uses to cause bending during needle insertion. Webster et al. [16] modeled needles with beveled tips as a nonholonomic kinematic systems and validated this model in simulated tissues. Further work shows that this nonholonomic model remains valid for other types of needle designs under certain circumstances, in this case a pre-curved section at the tip of the needle [17].

While the approach given in this paper extends the nonholonomic kinematic model developed by Webster et al., there are other techniques employed to steer needles, such as transverse and "tip/tilt" motion outside the tissue [5], duty cycling of the needle tip [4], or manipulation of the tissue itself [8]. Combinations of these steering methodologies might ultimately be used in a single, integrated setup, as proposed in [11] (see Figure 2 therein). In any such system, torsional dynamics – like those considered in this paper – will play a critical role in needle motion.

Kallem and Cowan [7] performed closed-loop control to a virtual plane inside the tissue via feedback linearization, assuming no torsional dynamics. Reed et al. [12] developed a model of torsional dynamics for a fixed length inside the tissue and performed open-loop torsional compensation during large needle tip reorientations. Kallem and Cowan noted that the controlled behavior of the needles differed from the theoretical predictions in a way that suggested torsional dynamics may have been playing a role. Reed et al.'s work later confirmed the significance of needle torsion on needle dynamics. The work presented in this paper builds on these two papers, incorporating both feedback control and a new model of torsional dynamics that include both continuous insertion and length-varying torsional dynamics inside and outside the tissue.

Other work incorporates needle and needle-tissue dynamics, but these have typically focused on tissue deformation and have approached the modeling problem using finite element methods [3] or simplified "virtual spring" models [5]. Here, we neglect tissue deformation, and focus our modeling effort on needle torsional wind-up, including the viscous drag between needle and tissue. Our approach uses a proper orthogonal decomposition, coupled with a Galerkin projection [6], [14], allowing us to side-step finite element techniques altogether. This approach gives us an exact, infinite dimensional representation of the system dynamics, which can then be systematically reduced to a manageable form by truncating higher-order terms in the infinite-dimensional expansion. Our work is analogous to a time-varying modal approach used for approximating the dynamics of a spacecraft antenna as it is extended [15].

II. Modeling

A. Previous Models of Tip-Steerable Needles

Given the body-fixed frame at the tip of the needle, as shown in Figure 1, the kinematic model developed by Webster et al. [16] describes the motion of the needle using the bicycle model with a fixed turning radius. The insertion velocity at the base of the needle prescribes the forward velocity of the bicycle and the rotational velocity at the base changes the orientation of the plane in which the bicycle travels.

This model can be succinctly described by the left-invariant vector field describing the motion of the needle tip in its body-fixed frame. The rigid body transformation

$$g = \begin{bmatrix} R & \mathbf{d} \\ \mathbf{0}^T & 1 \end{bmatrix} \in SE(3) \tag{1}$$

describes the orientation and position of the needle tip with respect to an inertial frame, where $R \in SO(3)$ and $\mathbf{d} \in \mathbb{R}^3$ are the rotation matrix and tip position respectively. The velocities in the body fixed frame are given as

$$\Omega_{\text{tip}} = \left(g^{-1}\dot{g}\right)^{\vee} = V_1 v + V_2 \omega, \tag{2}$$

where the twists associate with needle insertion velocity and tip rotational velocity are $V_1 = \kappa e_3 + e_4$ and $V_2 = e_6$, with e_i, $i = 1, \ldots 6$ the standard basis in $\mathbb{R}^6$. In most previous work on tip-steerable needles, it is assumed that the insertion and rotational velocities at base and tip were equal such that $v = u_1$ and $\omega = u_2$ with (u_1, u_2) the control inputs to the needle insertion robot. However real needles, for which we are twisting a long slender rod, the rotation at the base is coupled to the rotation at the tip through a dynamical system describing needle torsion. The work done by Reed et al. [12] demonstrates the need for torsional dynamics compensation, but their solution for torsion compensation assumes that the needle remains a fixed length inside the tissue, an assumption clearly violated during needle insertion. We build on Reed et al.'s result in the next section by incorporating the time-varying boundary conditions that result from continuous needle insertion.

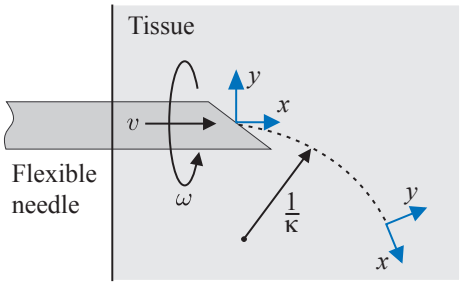

Fig. 1. The kinematic model used to represent the insertion of tip-steerable flexible needles, adapted from [16]. As the needle is inserted at velocity v, a tip asymmetry causes a lateral force that deflects the needle along a curved path of radius $1/\kappa$. Rotations about the tip with angular velocity ω reorient the bevel tip (Modified with permission from [10]).

B. Main Modeling Result: Time-Varying Torsional Dynamics

Our model of continuous needle insertion accounts for torsion both inside and outside the tissue as shown in Figure 2. We model the portion inside the tissue using a partial differential equation (PDE) that incorporates the rotational inertial forces of the needle, viscous drag forces between needle and tissues, and the shear forces due to needle properties. We model the portion outside the tissue as an ideal torsional spring whose spring constant is a function of the polar moment of inertia, J, the needle shear modulus, G, and the length outside the tissue, $L - l(t)$.

Using the Newton-Euler formulation for an infinitesimal portion of the needle inside the tissue, Reed et al. [12] derived a PDE in $\theta(x,t)$ a function of space and time,

$$\eta \frac{\partial^2 \theta}{\partial t^2} + \beta \frac{\partial \theta}{\partial t} - \kappa \frac{\partial^2 \theta}{\partial x^2} = \delta(x)\tau_{\text{in}}(t), \tag{3}$$

where β represents viscous damping (assumed to be uniform along the needle shaft), and η is rotational inertia. In Reed et al.'s model, it is assumed that the external torque on the needle is applied at the point that the needle enters the tissue, which is incorporated mathematically via the product of a spatial Dirac impulse function, $\delta(x)$, and the torque at the coupling between motor and the needle, $\tau_{\text{in}}(t)$.

Henceforth, our derivations deviate significantly from the previous work done by Reed et al. [12]. Fundamentally, the model from Reed et al. is only valid for a fixed distance of needle inside the tissue and assumes an exact measurement of the relative angle between base and tip. The subsequent

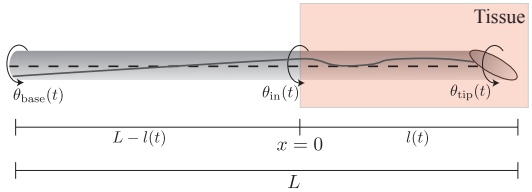

Fig. 2. The torsional dynamics of the needle is divided into the portion inside the tissue and outside the tissue. There is a time-varying changing boundary condition as the needle is inserted. The portion inside the needle is modeled through Newton force formulation resulting in a partial differential equation solved via modal methods. The portion outside the tissue is modeled as a torsional spring. Here, the dashed line represents an imaginary inscribed line with zero torsion. The gray line indicates the same inscribed line while the needle is under torsion.

derivation improves on this model in the following key respects: (1) we no longer model the system as a fixed length inside the tissue, (2) the system state is observed through limited measurements, and (3) we do not assume torque control at the point the needle enters the tissue.

First, we note that the torque at the motor–needle interface is exactly the same as the torque at the tissue boundary, since we assume a pure torsional spring for the portion of the needle outside the tissue. Hence, for the portion of the needle *inside* the tissue, we can still adopt the formulation in (3), where the spatial impuse is taken at $x = 0$. In other words, the torsional angle of the needle at the point of insertion into the tissue can be different from the angle at the motor, but the torque is the same all along the portion of the needle outside the tissue.

Because the needle length inside the tissue is changing, we cannot make the assumption that the modal solution is separable in both space and time. Instead, we can only assume that the mode shapes are functions of both space and time and the mode coefficients are functions of time:

$$\theta(x,t) = \frac{1}{2}\psi_0(x,t)q_0(t) + \sum_{k=1}^{\infty}\psi_k(x,t)q_k(t) + \sum_{k=1}^{\infty}\phi_k(x,t)p_k(t) \quad (4)$$

where

$$\left.\begin{aligned}\psi_j(x,t) &= \cos(\omega_j(t)x)\\ \phi_j(x,t) &= \sin(\omega_j(t)x)\end{aligned}\right\}, \quad \text{and} \quad \omega_j(t) = \frac{j\pi}{l(t)}. \quad (5)$$

A common practice in solving PDEs is to find the infinite dimensional solution to the PDE using the assumed modal solution and projecting back onto the first n-modes [1], [15]. The technique taken in this paper is one technique among a broader field of proper orthogonal decomposition and subsequent Galerkin projection [6], [13]. When the assumed solution is separable in space and time, where the mode shapes are function of the spatial variable and the mode coefficients are functions of time, the result of a Galerkin projection is an ordinary differential equation (ODE) in time. This method of model order reduction is particularly apropos when the system has a dissipative term causing exponential decay for states with high wavenumber.

For our system, the basis for the proper orthogonal decomposition are the torsional modes along the length of the needle as given in (5). As intimated previously, our system does not separate in space and time and we must perform the Galerkin projection and verify that each projection results in an ODE in time only; fortunately, the Galerkin projection for this system results in an ODE in time. To perform our Galerkin projection, we first substitute (4) into (3), and then project onto each mode shape. This rote computation is not included here in its entirety for brevity. However, the properties of key importance for simplification during the computations are related to the orthogonality conditions for the mode shapes, as shown in (6).

$$\begin{aligned}\int_{-l(t)}^{l(t)}\psi_k(x,t)\phi_j(x,t)dx &= 0 \quad \forall j,k>0.\\ \int_{-l(t)}^{l(t)}\psi_k(x,t)\psi_j(x,t)dx &= \begin{cases}2l(t), j=k=0,\\ l(t), j=k>0,\\ 0, j\neq k.\end{cases}\\ \int_{-l(t)}^{l(t)}\phi_k(x,t)\phi_j(x,t)dx &= \begin{cases}0, j=k=0,\\ l(t), j=k>0,\\ 0, j\neq k.\end{cases}\end{aligned} \quad (6)$$

The appropriate number of torsional modes to include in the truncated approximation of the system depends significantly on the tissue properties, needle properties, and control scheme employed. In Section IV, we compare and contrast through simulation and experimentation several model order truncations. Reed et al. analyzed a specific needle and tissue combination with experimentally computed damping and used Hankel singular values to determine an appropriate model order. For a general n-th order projection, the resulting ODE is of the form

$$\begin{bmatrix}M_1 & 0\\ 0 & M_2\end{bmatrix}\begin{bmatrix}\ddot{\mathbf{q}}\\ \ddot{\mathbf{p}}\end{bmatrix} + \begin{bmatrix}D_1 & 0\\ 0 & D_2\end{bmatrix}\begin{bmatrix}\dot{\mathbf{q}}\\ \dot{\mathbf{p}}\end{bmatrix} + \begin{bmatrix}K_1 & 0\\ 0 & K_2\end{bmatrix}\begin{bmatrix}\mathbf{q}\\ \mathbf{p}\end{bmatrix} = \begin{bmatrix}P\\ 0\end{bmatrix}\tau_{\text{in}}, \quad (7)$$

where the vectors $\mathbf{q}$ and $\mathbf{p}$ are the time-varying coefficients to the cosine and sine modes, respectively, as shown in (4).

We first note that the cosine and sine modes are decoupled, the sine modes are unforced, and the sine modes are naturally asymptotically stable. Thus, we can assume that for any experiment the sine modes are initially unexcited and can never be excited. From this point forward we will disregard the sine modes as both uncontrollable and always zero.

We model the portion of the needle outside the tissue as an ideal torsional spring, namely

$$\theta_{\text{base}} - \theta_{\text{in}} = \tau_{\text{in}}(t)\frac{L-l(t)}{JG}. \quad (8)$$

Here, the position at the insertion point of the needle, θ_{in}, is written in terms of the mode shapes and mode coefficients:

$$\theta_{\text{in}} = \theta(x,t)|_{x=0} \approx \frac{1}{2}q_0 + \sum_{k=1}^{n}\psi(0,t)q_k(t) = \underbrace{\begin{bmatrix}\frac{1}{2} & 1 & \cdots & 1\end{bmatrix}}_{C_0}\mathbf{q}. \quad (9)$$

The torque resulting from the rotational position at the base of the needle and the modal representation of the rotational position at the insertion is

$$\tau_{\text{in}} = -\frac{JG}{L-l(t)}C_0\mathbf{q} + \frac{JG}{L-l(t)}\theta_{\text{base}}, \quad (10)$$

where θ_{base} is the control input for subsequent control computations. The term $\frac{JG}{L-l(t)}$ can be thought of as the time-varying, lumped-parameter spring constant for the portion of the needle outside the tissue. Note that treating the portion of the needle outside the tissue as a torsional spring fails when the needle is fully inserted, which is demonstrated

by a singularity in the time-varying spring constant when $l(t) = L$.

Substituting the torque constraint from (10) into the ODE representing the torsional dynamics inside the tissue in (7) and neglecting the sinusoidal modes, the full torsional dynamics from base to tip is

$$M_1\ddot{\mathbf{q}}+D_1\dot{\mathbf{q}}+\left(K_1+\frac{JG}{L-l(t)}PC_0\right)\mathbf{q}=\frac{JG}{L-l(t)}P\theta_{\text{base}}. \quad (11)$$

We also note that the inertial forces associated with this system are quite small compared to the damping, shear, and control forces such that we can simplify the system to a coupled first order system,

$$\dot{\mathbf{q}}=\underbrace{-D_1^{-1}\left(K_1+\frac{JG}{L-l(t)}PC_0\right)}_{A(t)}\mathbf{q}+\underbrace{D^{-1}\frac{JG}{L-l(t)}P}_{B(t)}\theta_{\text{base}}. \quad (12)$$

Notice also that the velocity at the tip of the needle in the torsional dynamics, $\dot{\theta}(x,t)$, is equal to the body fixed rotational velocity, ω, given in equation (2). Thus, we compute

$$\begin{aligned}\theta_{\text{tip}} = \theta(x,t)|_{x=l(t)} &\approx \frac{1}{2}q_0+\sum_{k=1}^{n}\psi(l(t),t)q_k(t)\\ &=\underbrace{\begin{bmatrix}\frac{1}{2} & -1 & 1 & \cdots & (-1)^{n-1}\end{bmatrix}}_{C_\ell}\mathbf{q} \quad (13)\end{aligned}$$

and differentiate this to obtain

$$\omega=\dot{\theta}_{\text{tip}}=C_\ell\dot{\mathbf{q}}=\underbrace{C_\ell A(t)}_{C(t)}\mathbf{q}+\underbrace{C_\ell B(t)}_{D(t)}\theta_{\text{base}},$$

such that the final system can be written in a familiar linear, time-varying form:

$$\begin{aligned}\dot{\mathbf{q}}&=A(t)\mathbf{q}+B(t)\theta_{\text{base}}\\ \omega&=C(t)\mathbf{q}+D(t)\theta_{\text{base}}.\end{aligned} \quad (14)$$

C. Integration: Full Needle Dynamics

We now couple the torsional dynamics with the existing kinematic model. The velocity at the tip of the needle in the torsional dynamics, $\dot{\theta}(x,t)$, is equal to the body fixed rotational velocity, ω, given in equation (2). The full coupled form of the system can be described as

$$\begin{aligned}\Omega_{\text{tip}}&=V_1v+V_2\left(C(t)\mathbf{q}+D(t)\theta_{\text{base}}\right),\\ \dot{\mathbf{q}}&=A(t)\mathbf{q}+B(t)\theta_{\text{base}}.\end{aligned} \quad (15)$$

To compare controllers built on our general torsional model with previous methods, we choose local coordinates for the tip of the needle, namely Z-Y-X Euler angles (α,β,γ) for orientation and (x,y,z) for position as in Kallem and Cowan [7]. Following Kallem and Cowan further, we define the control task to be controlling the tip of the needle to an arbitrary plane in the tissue. With this control objective in mind, we can choose the local coordinates such that these local coordinates, $\mathbf{s}^T=\begin{bmatrix}x & y & z & \alpha & \beta & \gamma\end{bmatrix}$, are relative to the plane. That is, (y,z) are the position of the needle tip projected to the plane, x is the orthogonal distance from the plane, and α is the rotation of the needle about an axis orthogonal to the plane. The remaining parameters, β and γ, represent the pitch away from the plane and the rotation about the tip of the needle, respectively. The velocities in local coordinates can be related to the velocities in the body-fixed frame via the appropriate Jacobian,

$$\dot{\mathbf{s}}=J^{-1}(\mathbf{s})\Omega_{\text{tip}}. \quad (16)$$

Coupled with the torsional dynamics, the system can be represented as

$$\begin{bmatrix}\dot{\mathbf{s}}\\ \dot{\mathbf{q}}\end{bmatrix}=\begin{bmatrix}J^{-1}(s)V_1v+V_2\left(C(t)\mathbf{q}+D(t)\theta_{\text{base}}\right)\\ A(t)\mathbf{q}+B(t)\theta_{\text{base}}\end{bmatrix}. \quad (17)$$

For the task of controlling to a plane, Kallem and Cowan showed that (16) can be further reduced by "throwing away" the states (y,z,α), since they do not couple into the states (x,β,γ), and that $(x,\beta,\gamma)=(0,0,0)$ corresponds to the needle tip traveling in the desired plane [7]. Thus, we augment these three states with the torsional states, i.e. $\mathbf{r}=\begin{bmatrix}x & \beta & \gamma & \mathbf{q}^T\end{bmatrix}^T$. In these coordinates, the full needle model with reduced state and torsional dynamics included is

$$\begin{aligned}\dot{\mathbf{r}}&=\begin{bmatrix}v\sin(r_2)\\ \kappa v\sin(r_3)\\ -v\kappa\cos(r_3)\tan(r_2)+C(t)r_{4\cdots n}+D(t)\theta_{\text{base}}\\ A(t)q+B(t)\theta_{\text{base}}\end{bmatrix} \quad (18)\\ &=:f(\mathbf{r},\theta_{\text{base}},t).\end{aligned}$$

Here we have a nonlinear and time-varying system for which, in the following section, we devise a control strategy with the assumption that the orthogonal distance of the needle tip from the plane is our only measurement.

III. Control with Time-Varying Torsional Dynamics

Kallem and Cowan used feedback linearization to generate a system for which LQR/LQG control was implemented. Using the model in (18), an attempt to feedback linearize the kinematic states necessarily introduces a nonlinearity into the torsional states due to the manner in which the control input, θ_{base}, enters into the system

The approach we take here is to (1) linearize the system about the origin, (2) define a feedforward control to decouple the kinematic state from the torsional states, and (3) compute the infinite horizon LQR gain to optimally control the decoupled kinematic states to the plane. A key component in this control strategy is to show that the final control input ensures that the torsional state remains bounded for the duration of our insertion.

The linearization of the system about the origin is

$$\dot{\mathbf{r}}=\begin{bmatrix}0 & v & 0 & 0\\ 0 & 0 & \kappa v & 0\\ 0 & -\kappa v & 0 & C_lA(t)\\ 0 & 0 & 0 & A(t)\end{bmatrix}\mathbf{r}+\begin{bmatrix}0\\ 0\\ C_\ell B(t)\\ B(t)\end{bmatrix}\theta_{\text{base}}. \quad (19)$$

Let the control input be defined as

$$\theta_{\text{base}}=\frac{1}{C_\ell B(t)}\left(-C_\ell A(t)\mathbf{r}_{4\cdots n}+u_2(t)\right). \quad (20)$$

The first term decouples the kinematic and torsional states. This results in

$$\dot{\mathbf{r}} = \begin{bmatrix} 0 & v & 0 & 0 \\ 0 & 0 & \kappa v & 0 \\ 0 & -\kappa v & 0 & 0 \\ 0 & 0 & 0 & \overline{A}(t) \end{bmatrix} \mathbf{r} + \begin{bmatrix} 0 \\ 0 \\ 1 \\ \frac{1}{C_\ell B(t)} B(t) \end{bmatrix} u_2(t), \quad (21)$$

where $\overline{A}(t) = A(t) - \frac{1}{C_\ell B(t)} B(t) C_\ell$. The first three states of the decoupled system are controllable and we implement a controller of the form

$$u_2(t) = \begin{bmatrix} k_1 & k_2 & k_3 & 0 & \cdots & 0 \end{bmatrix} \mathbf{r}, \quad (22)$$

where the gain is from the infinite horizon LQR solution to minimize the cost function

$$J = \int_{t_0}^{\infty} \mathbf{r}_{1\cdots3}^T(\tau) Q \mathbf{r}_{1\cdots3}(\tau) + R u_2^2(\tau) d\tau. \quad (23)$$

Heretofore we have assumed full state feedback, but in practice, we are only able to measure a scalar output: the distance from the desired plane. Fortunately, a straight forward calculation can be used to verify observability of the system analytically by reconstructing the state from the output and its first $n-1$ derivatives (the proof is omitted here due to space constraints). So, in our simulations and experiments we use a Kalman filter to estimate the states of the linearized system (19), and apply state feedback on this estimate, as is standard practice.

IV. Experimental Results

Here we present simulations and experiments to demonstrate that the modeling and control methods described herein provide an improvement over existing control methods which do not compensate for torsional dynamics during insertion. In lieu of a systematic approach for model reduction (e.g. based on the Hankel singular values) for this LTV system, we compare control efficacy based on models of different orders in an extensive set of simulations. We consider both deterministic simulations assuming full state access, as well as simulations assuming stochastic dynamics with output feedback. In addition, we present pilot experiments on our needle insertion robot. In all simulations, we use a 25^{th} order torsional truncation as the "real" system. In both simulations and experiments we show results associated with representing the torsional dynamics with 1, 5, and 25 truncated states. Table I lists parameters used for all simulations and experiments. Density and polar moment of inertia were computed from manufacturer specifications. Shear modulus, viscous drag between needle and tissue, and radius of curvature were determined experimentally.

Parameter	Value
Density (ρ)	6.45×10^3 $\frac{\text{kg}}{\text{m}^3}$
Polar moment of inertia (J)	2.3572×10^{-14} m^4
Shear modulus (G)	2.72×10^{10} Pascals
Viscous drag (β)	2.23×10^{-2} N$\cdot$m$\cdot$s
Radius of curvature ($1/\kappa$)	0.122 m

TABLE I

Parameters used in simulations and experiments shown in Figure 3 and Figure 4.

A. Numerical simulations suggest that higher order models can improve robustness to noise

We conducted two series of simulations to identify the effect of model order on control of the needle tip to the plane: 1) deterministic control with full state access and 2) control of a noisy system with reduced measurements. The deterministic simulations allow us to identify the best possible performance for our control method. The noisy system and reduced measurements are more indicative of the conditions experiences during real experimentation. Neither simulation is an exact representation as we simulate the "real"system with a 25 state representation of the torsional dynamics. A higher order model could have been generated at the cost of prohibitively long Galerkin projections in Mathematica, and since we found that the fifth order modal model almost exactly reproduces the twenty-fifth order model, we are reasonably confident that 25 modes are more than sufficient to capture the dynamics for simulations.

Figure 3(A) shows the deterministic simulation results. Interestingly, with full state access there is very little difference between the various model orders of torsional dynamics. This may indicate that the windup outside the tissue is the dominant effect for the chosen simulation parameters, thus even one modal state captures the salient dynamics. Figure 3(B-D) shows the simulation results of a noisy system with output feedback (1000 simulations for each model order). These results indicate that all controllers (based on different order modal models) exhibit similar rise times, but the overshoot and final settling time improves with increased model order.

B. Physical experiments suggest that one modal state is sufficient to enhance control

We conducted preliminary experiments with our needle insertion robot and artificial tissue (plastisol). The experimental setup consists of an industrial PC running a modified Ubuntu installation with RTAI realtime extensions, stereo cameras for needle tip triangulation, and our needle insertion robot (the system is similar to that of Kallem and Cowan [7]). For these experiments we performed a single insertion without rotating at the base and fit a circle to the recorded tip measurements to identify the radius of curvature. Values for density, shear modulus, and viscous drag were obtained by dimensionally scaling the reported results in [12] based on our needle diameter of 0.635 mm.

Figure 4 shows the results of 5 experiments for each model order. These preliminary experiments show very little difference between each of estimator/controller pairs based on the different model orders. We suspect that some of this is due to the model parameters being inaccurate and in future experiments we will characterize the model parameters explicitly for each needle/tissue pairing, rather than relying on previous results.

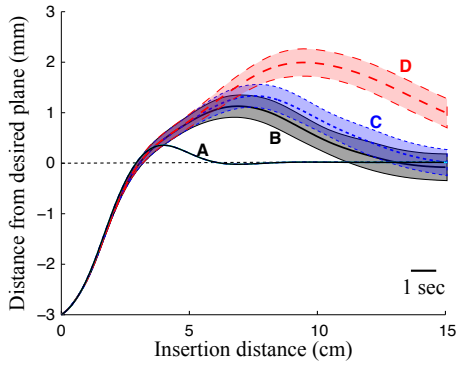

Fig. 3. Simulation results for 15 cm insertions at $v = 1$ cm/s. All simulations assume a "real" system of 25 modal states, but the feedback control is based on either 1, 5, or 25 modal states. **(A)** Deterministic simulation using a control signal based on 25 modal states and full-state feedback. **(B, C, D)** Estimator-based output feedback control assuming process and sensor noise. The mean trajectory (center line, solid or dashed) and standard deviation (shaded regions) for 1000 trials of each model order are shown: **(B)** The 25 modal state model, **(C)** the 5 modal state model, and **(D)** the 1 modal state model. Here we see that more torsional states can improve performance when using estimator-based output feedback.

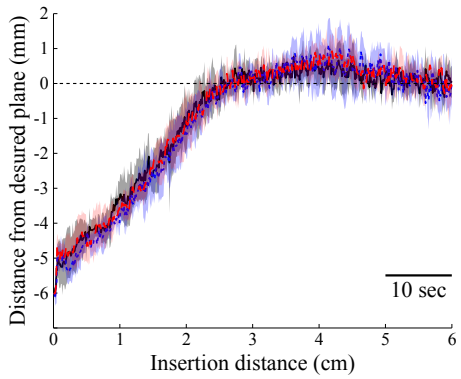

Fig. 4. Physical experiments for 6 cm insertions at $v = 1$ mm/s. These results show little difference between different model orders, but categorical improvement over previously reported experimental control results [7]. The mean trajectory and standard deviation for 5 trials of each model order are shown, with an initial error of 6 mm from the desired plane: 1 modal state (red), 5 modal states (blue), and 25 modal states (black). Note scale differences when comparing with Figure 3.

V. Discussion

A. Significant improvement over previously reported experimental results

This paper presents a new model for torsional dynamics, that takes into account time-varying boundary conditions. The primary conclusion from our experimental results is that the incorporation of these time-varying dynamics into a closed-loop control scheme significantly improves performance over the purely kinematic control method used previously. Specifically, the experimental trials reported in Kallem and Cowan [7], which did not incorporate torsional dynamics into the control algorithm, required an insertion distance of about 8 cm to recover from a 3 mm initial error from the desired plane. Here we show experimental convergence to the plane in approximately 2.5–3 cm of insertion despite a larger initial error from the plane of 6 mm. Future experiments should evaluate both algorithms using the exact same tissue and needle for a more equitable comparison.

B. Faster than expected convergence in physical experiments

Interestingly, the model order did not seem to have a great impact on the rate of convergence for the physical experiments. This may indicate that our noise parameters in the simulations were significantly greater than those of the real system. To examine this more carefully requires a careful system identification of noise and system parameters, which will be the subject of future studies.

VI. Acknowledgments

The authors thank T. Wedlick, M. Moses, K. Reed, E. Roth, and A. Okamura for valuable discussions and input during the development of this work.

References

[1] L. Chen and X. Yang. Transverse nonlinear dynamics of axially accelerating viscoelastic beams based on 4-term galerkin truncation. *Chaos, Solitons & Fractals*, 27(3):748–757, 2006.

[2] N. J. Cowan, K. Goldberg, G. S. Chirikjian, G. Fichtinger, R. Alterovitz, K. B. Reed, V. Kallem, W. Park, S. Misra, and A. M. Okamura. Robotic needle steering: Design, modeling, planning, and image guidance. In J. Rosen, B. Hannaford, and R. Satava, editors, *Surgical Robotics – Systems, Applications, and Visions*, pages 557–582. Springer, 2011.

[3] S. DiMaio and S. Salcudean. Needle insertion modeling and simulation. *IEEE Trans. Robot. Automat.*, 19:864–875, 2003.

[4] J. Engh, D. Minhas, D. Kondziolka, and C. Riviere. Percutaneous intracerebral navigation by duty-cycled spinning of flexible bevel-tipped needles. *Neurosurgery*, 67(4):1117, 2010.

[5] D. Glozman and M. Shoham. Image-guided robotic flexible needle steering. *Robotics, IEEE Transactions on*, 23(3):459–467, 2007.

[6] P. Holmes, J. Lumley, and G. Berkooz. *Turbulence, coherent structures, dynamical systems and symmetry*. Cambridge Univ Pr, 1998.

[7] V. Kallem and N. J. Cowan. Image guidance of flexible tip-steerable needles. *IEEE Trans. Robot.*, 25:191–196, 2009. NIHMS192987.

[8] V. G. Mallapragada, N. Sarkar, and T. K. Podder. Robot-assisted real-time tumor manipulation for breast biopsy. *IEEE Trans. Robot.*, 25(2):316–324, 2009.

[9] S. Okazawa, R. Ebrahimi, J. Chuang, S. E. Salcudean, and R. Rohling. Hand-held steerable needle device. *IEEE/ASME Trans. Mech.*, 10(3):285–296, 2005.

[10] W. Park, K. B. Reed, A. M. Okamura, and G. S. Chirikjian. Estimation of model parameters for steerable needles. *Proc. IEEE Int. Conf. Robot. Autom.*, pages 3703 –3708, may. 2010.

[11] K. B. Reed, A. Majewicz, V. Kallem, R. Alterovitz, K. Goldberg, N. J. Cowan, and A. M. Okamura. Robot-assisted needle steering. *IEEE Robot. Autom. Mag.*, 18(4):35–46, Dec. 2011.

[12] K. B. Reed, A. M. Okamura, and N. J. Cowan. Modeling and control of needles with torsional friction. *IEEE Trans. Biomed. Eng.*, 56(12):2905–2916, Dec. 2009. NIHMS192959.

[13] C. Rowley. Model reduction for fluids, using balanced proper orthogonal decomposition. *International Journal of Bifurcation Chaos in Applied Sciences and Engineering*, 15(3):997–1014, 2005.

[14] K. Sze, S. Chen, and J. Huang. The incremental harmonic balance method for nonlinear vibration of axially moving beams. *Journal of sound and vibration*, 281(3-5):611–626, 2005.

[15] L. Wang, Z. Hu, Z. Zhong, and J. Ju. Hamiltonian dynamic analysis of an axially translating beam featuring time-variant velocity. *Acta Mechanica*, 206(3):149–161, 2009.

[16] R. J. Webster III, J. S. Kim, N. J. Cowan, G. S. Chirikjian, and A. M. Okamura. Nonholonomic modeling of needle steering. *Int. J. Robot. Res.*, 25(5/6):509–526, May 2006.

[17] T. Wedlick and A. Okamura. Characterization of pre-curved needles for steering in tissue. In *Engineering in Medicine and Biology Society, 2009. EMBC 2009. Annual International Conference of the IEEE*, pages 1200 –1203, sept. 2009.

[18] A. Wood. New method of treating neuralgia by the direct application of opiates to the painful points. *Edin. Med. Surg. J.*, 82:265–281, 1855.